Multiple Diving Waves and Steep Velocity Gradients in the Western Taiwan Coastal Plain: An Investigation Based on the TAIGER Experiment

by Bor Shouh Huang, Chien Ying Wang, David Okaya, Shiann-Jong Lee, Ya-Chuan Lai, Francis T. Wu, Wen-Tzong Liang, and Win-Gee Huang

Abstract   Seismic data collected during explosion experiments performed as part of the TAiwan Integrated GEodynamics Research (TAIGER) project provide an excellent opportunity to obtain high-resolution images of the structure of the crust and upper mantle beneath Taiwan. The most significant feature observed at near-source stations located on the western coastal plain in Taiwan is high-energy later arrivals. These high-amplitude multiples almost completely mask the lower-amplitude signals (seismic refraction and wide-angle reflection) from the deep crust. The later arrivals are identified as free-surface-reflected multiples. The nature and generation of these high-energy, multiple diving waves are demonstrated using synthetic examples. Their generation requires the presence of a steep velocity gradient in the shallow crust. A detailed analysis of the observation data provided information on the velocity gradients in this region. An accurate layer-velocity model, including the boundary orientation and its depth, and velocity gradient, was constructed based on a 1D waveform simulation and 2D seismic raytracing modeling for travel times. The present results indicate that the thick sediment in the survey area dips shallowly to the east, has a surface *P*-wave velocity of 1.76 km/s, and an average velocity gradient of about 0.72/s from the surface to 3.0-km depth. The thick sediment of the 2D model shows lateral variations in velocity gradient, increasing from west to east. This velocity model may provide useful information for future data processing to reduce multiple diving waves with the aim of enhancing the deep-surface refraction/reflection signal. The velocity gradient calculated for the thick sediment of the western coastal plain may require a revision of the regional seismic velocity model developed for southwestern Taiwan, to improve the accuracy of regional hypocenter determinations, and to predict the strong ground motions produced by large earthquakes beneath this region.

Introduction

The collision of the Luzon arc with the southeast China continental margin, which formed Taiwan within the past 4–5 million years, is recognized as the most active arc-continent collision zone worldwide (Wu *et al.*, 2009). In 2005, the TAiwan Integrated GEodynamics Research (TAIGER) experiment, an international project that sought to study the Taiwan orogeny, was performed to test existing geodynamical models, and to develop new models based on geophysical imaging, earthquake recording, and subsequent geodynamic analyses (Wu *et al.*, 2007; Okaya *et al.*, 2009). In early 2008, dense seismic refraction and wide-angle reflection explosion experiments were successfully conducted along two east–west profiles across the northern and southern parts of Taiwan. Seismic sources were exploded with a charge of up to 3000 kg. The resulting seismic waves propagated over distances greater than 300 km and were well-recorded by regional seismic stations (Wang *et al.*, 2008). The seismic signals recorded along the seismic refraction and wide-angle reflection sections are highly spatially coherent. These observations provided an excellent opportunity to obtain high-resolution 2D images of the structure of the crust and upper mantle beneath Taiwan.

The southern profile, which crosses the western coastal plain of Taiwan, consisted of densely deployed seismic stations at intervals of about 200 m (Fig. 1). Most of the recorded seismograms show a high-resolution signal in the first arrival. However, in the western portion of this seismic section, the most significant feature of those seismograms is the presence of high-energy later arrivals, which are neither simple refractions nor reflections. In fact, these signals are so dominant that they control the entire character of the seismograms obtained throughout the western plain and obscure
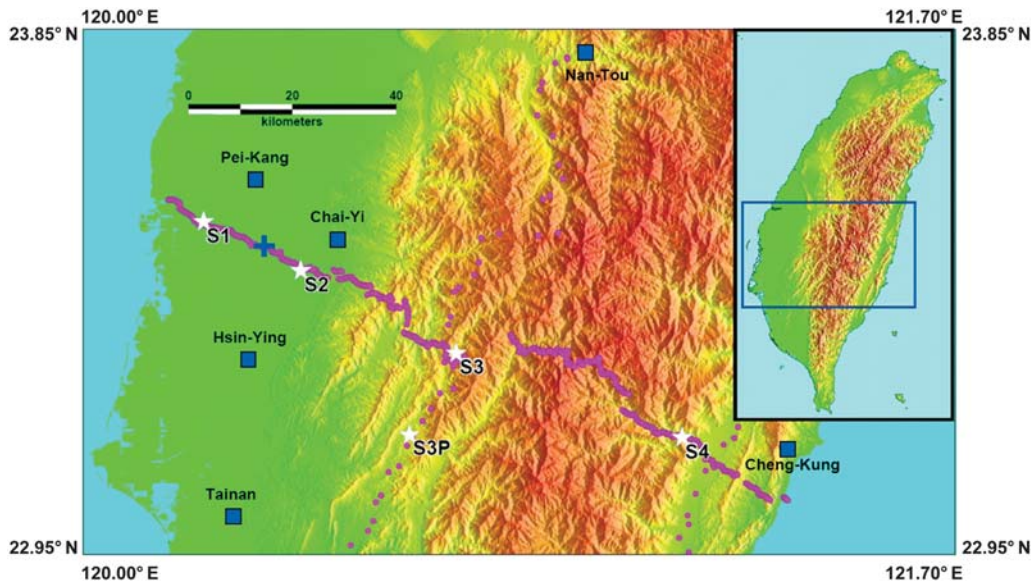
Figure 1.   Location of the TAIGER seismic profile in southern Taiwan. White stars, the shot points; pink circles, stations along the seismic profile.

any refraction and reflection signals from the deep crust. These later arrivals are generally not visible on other shot records of the TAIGER experiment (Huang *et al.*, 2008). Similar observations have been reported previously from the Imperial Valley of California and from the Bengal basin of India, and were interpreted as free-surface multiples (or multiple diving waves) that belong to the family of free-surface reflections that have dived more than once within the crust before reaching the free surface (McMechan and Mooney, 1980; Sarkar *et al.*, 1995).

In this study, we revisit this issue with the aim of identifying the origin of these high-energy later arrivals recorded throughout the western coastal plain of Taiwan, in order to understand their propagation behavior and to explore their application in terms of determining the velocity structure and predicting future ground motions. The results indicate that the later arrivals are multiple diving waves generated by steep velocity gradients in sediment layers. An accurate 2D layer-velocity model, including the velocity gradient, was constructed based on 2D seismic-raytracing modeling. The new model reveals an east-dipping sediment layer with a steep velocity gradient in the shallow crust. This gradient, described here for the first time, has an effect on wave propagation. The gradient may result in enhanced high-frequency ground motions, produce extended periods of strong ground shaking, and may complicate the interpretation of seismic signals.

Data

The southern profile of the TAIGER wide-angle reflection and refraction experiment was surveyed on 27–29 February 2008. This profile crosses Taiwan from west to east (Fig. 1). TAIGER data were recorded using autonomous one-component digital seismic stations (Texans [REFTEK-125 s] from the University of Texas at El Paso). These 604 instruments were deployed along the 134-km-long main TAIGER southern Taiwan profile at intervals of about 200 m. All stations along the section recorded five shots, with four shots placed in-line and one shot placed off-line with a charge of 3000 kg (S3P in Fig. 1). The Chia-Nan Plain, which is widely covered by a great thickness of recent alluvium, is located in the western portion of the seismic profile (Fig. 1). In the plain region, two shots (S1 and S2) were exploded with charge sizes of 1000 and 750 kg, respectively. Both of the explosion sources radiated strong seismic energy.

Figure 2a shows the automatic gain control seismic section from shot point S2. The signals received from east and west of the shot point are different in terms of travel times and the amplitudes of the later phases. These differences are consistent with the site condition, as shown in the geological cross section in Figure 2b. In addition to clear first arrivals, the dominant feature of the seismic wave fields across the plain area is the presence of distinct, high-amplitude later phases. In the plain area, the sections recorded from S1 are similar to those from S2 in terms of the high-energy later arrivals (Fig. 3a,b). These strong phases appear to have traveled subparallel to the first arrivals. The travel-time curves for these waves, unlike those for the head waves, are not straight, but are concave downward.

The data analyzed in this study (as shown in Fig. 3a,b) span a seismic profile with distance of 40 km. This profile includes a reversed profile (20 km) from both shot points S1 and S2 (Fig. 1). Both of these sections are suitable for detailed analysis because the later arrivals are more prominent than in the other profiles, thereby providing the best information with which to investigate the origin and propagation characteristics of these waves. Both sections were recorded
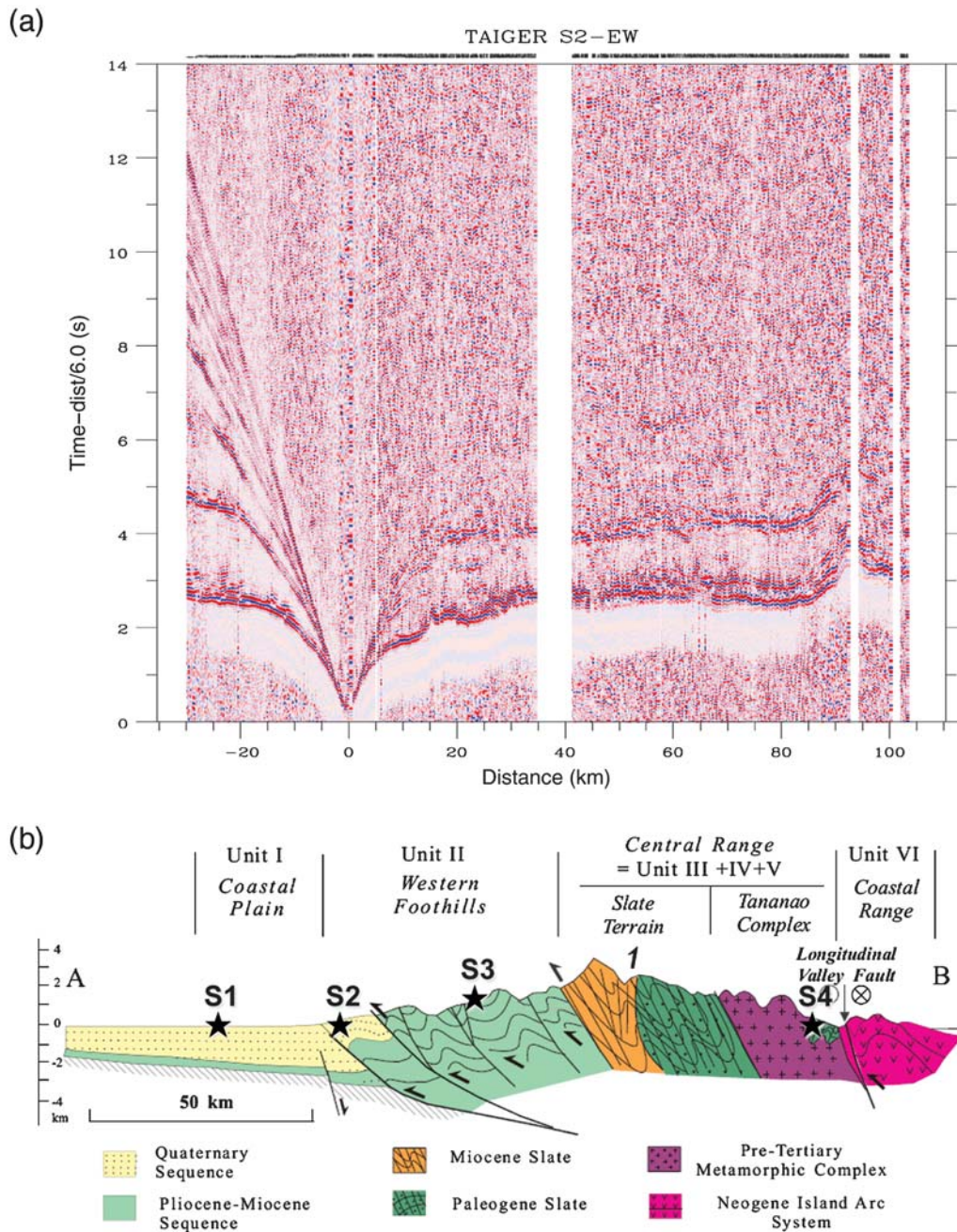
Figure 2. Trace of the normalized record section of shot point S2 located at a distance of 0 km. (a) A velocity of 6.0 km/s was used to reduce the time section. (b) A simplified geological cross section of the Taiwan mountain belt, parallel to the seismic profile (Teng, 1990). The locations of shot points (Fig. 1) are projected onto the cross section.

by identical instruments from two individual shots and the recording sites were identical for both shots. This uniformity helps in correlating arrivals across the profile and in determining the origin of complex waveforms. For example, Figure 4a,b shows two seismograms selected from the station located closest to the middle point of the reversed profile. The inconsistent first arrivals indicate lateral variations in the seismic structure beneath the profile. Although both waveforms show complex and high-frequency components, the seismic profile in Figure 3a shows that these later phases

can be traced as coherent signals over long distances, thereby excluding an origin as complex waveforms generated by local site effects or random scatter. For both seismic sections in Figure 3a,b, the first arrivals form a smooth curve with respect to distance, indicating a continuously increasing velocity with increasing depth in the thick sedimentary layer. Far from the shot point, the first arrivals define as straight lines, indicating refraction from a deep layer, with an apparent velocity of approximately 5.5 km/s. In addition to the clear first arrivals, both profiles are characterized by several distant
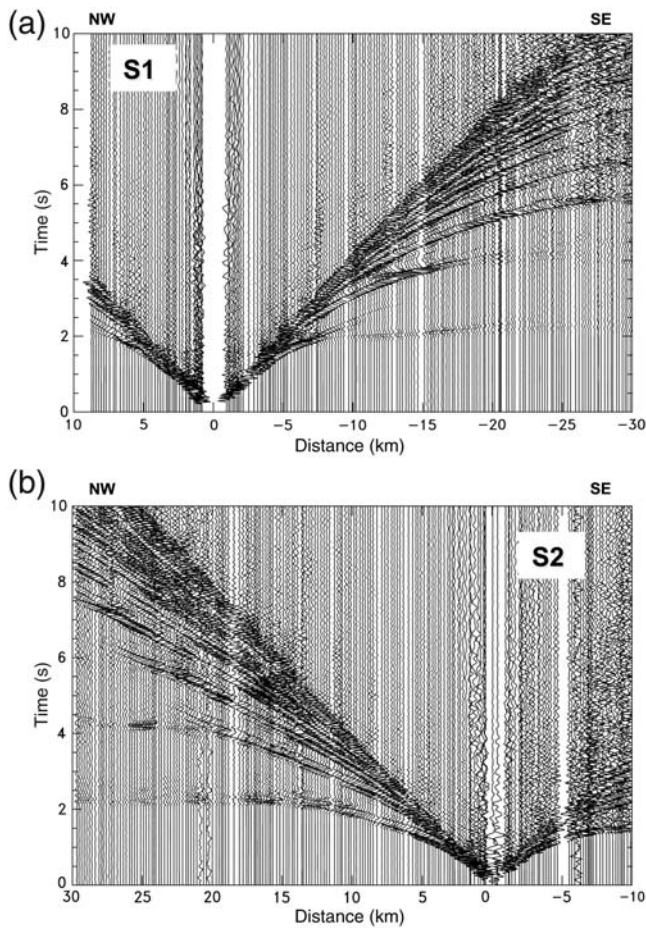
Figure 3. Shot-offset seismic sections for shot points (a) S1 and (b) S2. The distance shown in both seismic sections increases from the shot point (0 km) toward the northwest. A velocity of 5.5 km/s was used to reduce both time sections.

later arrivals (Fig. 3a,b). The travel times of the later, high-amplitude phases show a similar pattern for both the S1 and S2 shots, indicating little lateral variation in velocity layering beneath this region. Modeling of these later arrivals is an important aspect of our analysis in terms of verifying these phases, as this constrains the model beyond what would be possible from an analysis of first arrivals alone.

Analysis and Results

First, we fitted the straight-line portions of first-arrival travel times from both seismic profiles as boundary refraction waves, to obtain a conventional solution for a dipping constant-velocity layer. Limited by the spatial extent and the lack of clear head waves, travel times as straight lines can be selected over shorter distances, and average velocities were selected for direct waves. From the seismic profile of shot S1 (Fig. 3a), the crossover distance can be picked at 7 km. This observation can be reasonably fitted using a two-layer model with *P*-wave velocities of 2.14 km/s in the top layer and 5.5 km/s in the bottom layer, and a near-horizontal interface

with a thickness of 1.5 km, as estimated from the S1 shot profile. From the seismic profile of shot 2 (Fig. 3b), the crossover distance can be picked at 11 km. This observation can be fitted using a two-layer model with *P*-wave velocities of 2.75 km/s in the top layer and 5.5 km/s in the bottom layer, and a near-horizontal interface with a thickness of 1.8 km, as estimated from the S2 shot profile. It indicated that an east-dipping layer and the lower boundary were considered as the sedimentary basement in this region. However, this proposed layer structure has not been supported by previous studies. Furthermore, the travel-time curves of the proposed layer model are inadequate in representing the observed, smoothly curving travel time of this seismic profile (Fig. 3). This finding indicates that this approach is not suitable for the present observations.

Next, we selected a regional crustal model of southwestern Taiwan, as proposed by Chen (1995), as an initial model for the travel-time and waveform modeling. The model was constructed by fitting the travel times of local events and has been routinely used by the Central Weather Bureau (CWB) to locate earthquakes. This model has eight layers for the crust (35 km in total thickness), and *P*-wave velocities of 3.49 km/s at the surface and 5.7 km/s at a depth of 10 km (labeled Model-CWB in Fig. 5). Using this model, we first tried to generate the later arrivals that followed the primary phases. Based on this 1D-layer model, we computed the later arrivals by generating synthetics using the WKBJ method (Chapman, 1978) to infer the velocity structure of the sedimentary layer in the profile. The WKBJ method is particularly suitable for reliable modeling of the amplitude of the present dataset, including multiples, because these non-geometrical signals can be simulated to evaluate the shallow structure of this region.

Based on Chen's (1995) model, synthetic modeling was performed to generate synthetic seismograms and travel curves of the primary and later phases. The modeling results are shown in the upper panel of Figure 6a; the corresponding ray diagram is shown in the lower panel. According to this model, the later phases can be generated only by layer reflection waves. Clearly, the amplitudes of these later phases are too small and cannot satisfy the features of the later arrivals in the observed section (Fig. 3). Therefore, we modified the model by gradually increasing the velocity gradient in each layer and by making corresponding reductions in the velocity contrast across the interfaces.

Following these modifications, the generated synthetic seismograms (Fig. 6b) possess the main features of the observed seismograms from shot points S1 and S2 (Fig. 3). The computed travel times (Fig. 6a,b) have different shapes. The travel-time curves of the constant-layer model are concave upward (Fig. 6a), whereas those of the gradient model are concave downward (Fig. 6b). In general, a travel-time curve with a concave-upward shape is considered to indicate a refracted reflection wave, whereas that with a concave-downward shape is considered a reflected refraction wave (Meissner, 1965). Figure 6b (lower panel) shows a ray diagram of
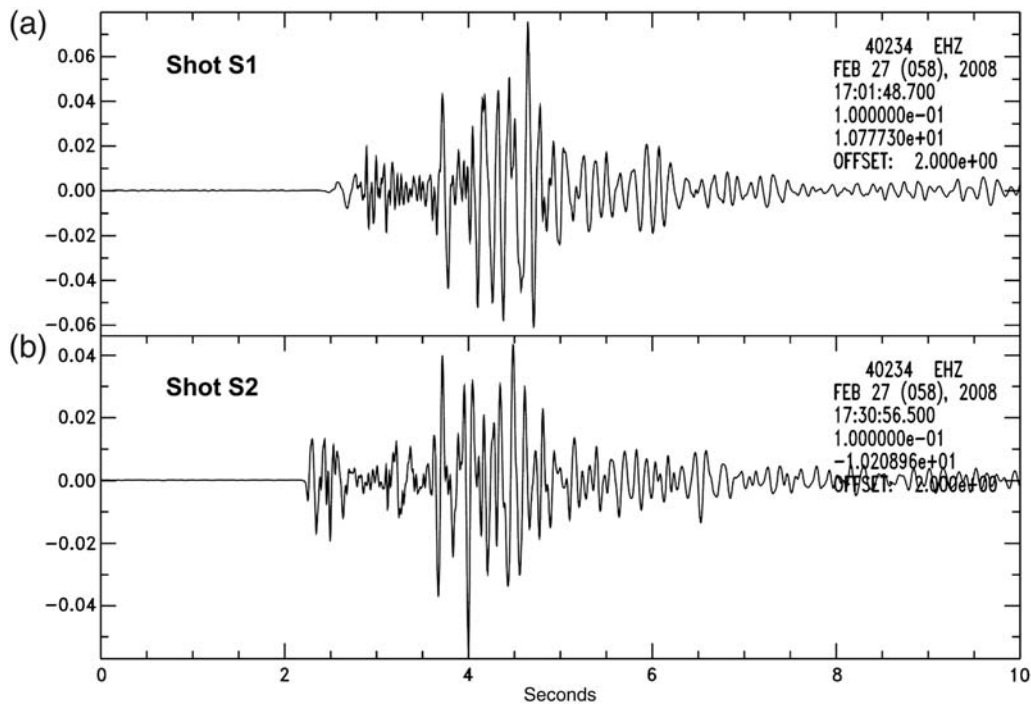
Figure 4. Vertical seismograms recorded by station 40234 for shot points (a) S1 and (b) S2. The station is located at similar distances from S1 and S2 (blue cross in Fig. 1).

the later phases according to this gradient-velocity model. The later phases from the constant-velocity-layer model are the layer-reflected waves and their multiples (lower panel in Fig. 6a). The later phases from the gradient-velocity model are the free-surface-reflected waves and their multiples (lower panel in Fig. 6b). Theoretically, free-surface multiples could exist in either model; however, these amplitudes should decay quickly with respect to travel distance because the energy is continuously leaked during the multiple internal reflections. In the case of steep velocity gradients in the layers, all of the seismic energy is curved upward, with the result that these phases are prominent on seismograms. We verified that the later-arrival energy observed over southwestern Taiwan is related to diving waves that were multiply reflected at the free surface.

The model employed to generate the travel-time curves and synthetic seismograms of Figure 6b was a 1D model with manual updating to fit the travel-time curves of the observed seismograms of TAIGER shots S1 and S2. The seismic velocity profile of this model is shown as a blue curve in Figure 5 (labeled Model-1D). The computed travel-time curves fitted to the first arrival and its later phases are plotted with seismic profiles in Figure 7. The two seismic sections, recorded from two shots conducted at each end of the profile, are reasonably fitted by the computed travel-time curves of this horizontal layered model. The resulting model (Fig. 5) shows a steep velocity gradient in the uppermost 3 km. The upper layer has a *P*-wave velocity of 1.76 km/s at the surface and a velocity gradient of 0.72/s. The second layer

has a slight velocity jump to 4.12 km/s at its uppermost boundary and extends to 7-km depth, with a velocity gradient of 0.33/s. The later arrivals were unaffected by changes in the velocity model parameters for depths greater than this lower boundary, indicating that the diving waves are restricted to the boundary layers above. Both of these layers can be considered as Cenozoic sedimentary rock, which extend to depths in excess of 6 km (Lin *et al.*, 2003).

Although the proposed 1D gradient velocity model was successful in reproducing the concave-downward multiples and was reasonable in fitting the observed seismic profiles, the fitting consistency differed along each of the seismic profiles. The fit of the first arrival and its first multiple from shot S1 were better than that for shot S2. Furthermore, the high-order multiples from both shots were not well fitted by this model. This result raises the possibility of a dipping layer boundary and lateral heterogeneity of seismic velocity in the sediment. To obtain an optimal model to fit profiles from both shots, a forward 2D seismic-raytracing code (RAY84; Luetgert, 1988) was employed to compute travel times to fit both first arrivals and multiples from the two seismic profiles (Fig. 3). The search begins from a 1D model, such as Model-1D in Figure 5, and the depth of the sediment boundary is systematically varied in a 2D model to represent a simple dipping layer. The computed travel-time curves for shots S1 and S2 using an east-dipping layer were consistently well fitted to the first arrivals of both seismic profiles (Figs. 8 and 9). However, the high-order multiples were not affected by changes in the orientation and depth of the boundary.
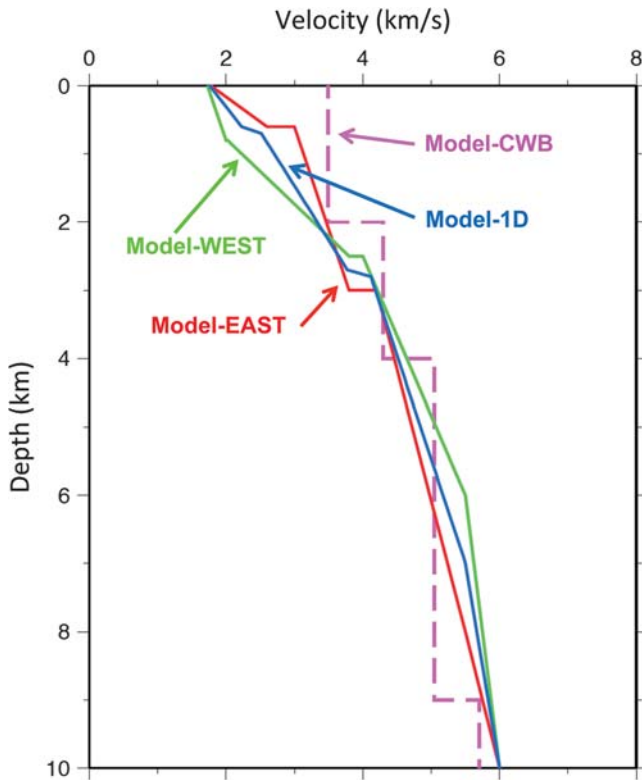
Figure 5. One-dimensional *P*-wave velocity profiles used in this study. Pink dashed line, the regional crustal model proposed by Chen (1995), which is employed by the CWB to locate earthquakes in the southwestern Taiwan region (Model-CWB); blue solid line, a layered velocity model with a velocity gradient, which provides the best-fit 1D model for the TAIGER explosion observations from shots S1 and S2 (Model-1D); the green and red solid lines represent velocity profiles of the western and eastern boundaries of the final determined 2D model of this study (Model-WEST and Model-EAST, respectively). The 2D model proposed in this study was constructed by a linear interpolation of the two 1D velocity profiles.

To fit the travel-time curves of multiples, we layered the sediment and provided lateral variations in seismic velocities and boundary depths within each layer of sediment. The computed travel times of multiples were best fitted to the seismic profiles when using a model with increasing seismic velocity and increasing velocity gradient from west to east. In addition, this model required a thicker layer of shallow sediment in the west. After manually tuning many of the possible 2D models to reduce the travel-time residuals, the first arrivals and multiples of the two profiles are commonly fitted by a single 2D model. The 2D model (Fig. 10) was represented as a linear interpolation of two 1D velocity models (Model-WEST and Model-EAST in Fig. 5) at either end of the model. The thick sediment was divided by an east-dipping boundary near a depth of 3 km. The upper 3 km of sediment had a higher velocity gradient than that below 3 km. In this model, the upper 3 km of sediment shows lateral variations, with higher seismic velocities and gradients in the

east and a thicker layer of shallow sediment in the west. According to this model, the computed seismic travel times fitted not only the first arrivals but also the high-order multiples for both seismic profiles (upper panels in Figs. 8 and 9).

Discussion

The multiple diving waves are observed because of the favorable geological setting of the survey region. A thick sediment layer with a steep velocity gradient is necessary to trap this phase. The resulting model (Fig. 10) shows a steep velocity gradient in the top layers of the southwestern Taiwan coastal plain. In this study, we showed how to identify and distinguish multiple diving waves from the primary phases, based on the characteristics of their arrival-time patterns. Phase identification is a basic component of seismic data processing. The primary phases (e.g., refraction, reflection, and diffraction) and converted waves are usually used to construct a seismic profile. In the western coastal plain of Taiwan, observations from a seismic explosion survey (e.g., TAIGER shot S2; Fig. 2) suggest that the primary phases may be embedded within the multiple diving waves. It is difficult to identify primary phases from such a seismic profile. Thus, multiple diving waves are considered as noise in standard data-processing procedures that seek to retrieve deep refracted and reflected signals. The present results indicate that the multiple diving waves have apparent velocities and travel-time patterns that differ from those of the primary phases. On the other hand, based on their propagation characteristics, the use of a velocity filter and other data-processing tools may help to reduce the amplitudes of multiple diving waves and thereby enhance the primary phases in future data processing. Furthermore, the multiple diving waves can be utilized as seismic signals to construct an accurate gradient-velocity model at shallow layers in compiling a regional crustal model.

The southwestern Taiwan coastal plain is an area of high earthquake activity and is at risk of severe earthquake-related damage. In terms of mitigating seismic hazards, an accurate seismic model is required to determine earthquake locations and to predict the intensity of ground motions likely to be associated with future events. The regional model proposed by Chen (1995) has been employed by the CWB for routine earthquake locations (Fig. 5). This model has proved to be successful in locating earthquakes in the region, as is earthquake waveform modeling at low frequencies (Huang, Chen, *et al.*, 1996). However, this model is inverted by local earthquake travel times that are largely unaffected by the shallow structure. In fact, the model proposed by Chen (1995) contains no information on velocity gradients in shallow layers. However, according to the results of numerical modeling performed as part of the present study, the repeat arrivals from the multiple diving waves may act to extend the duration of ground motions and enhance the amplitude. Numerical simulations based on the model developed by Chen (1995) may underestimate the ground amplitude and
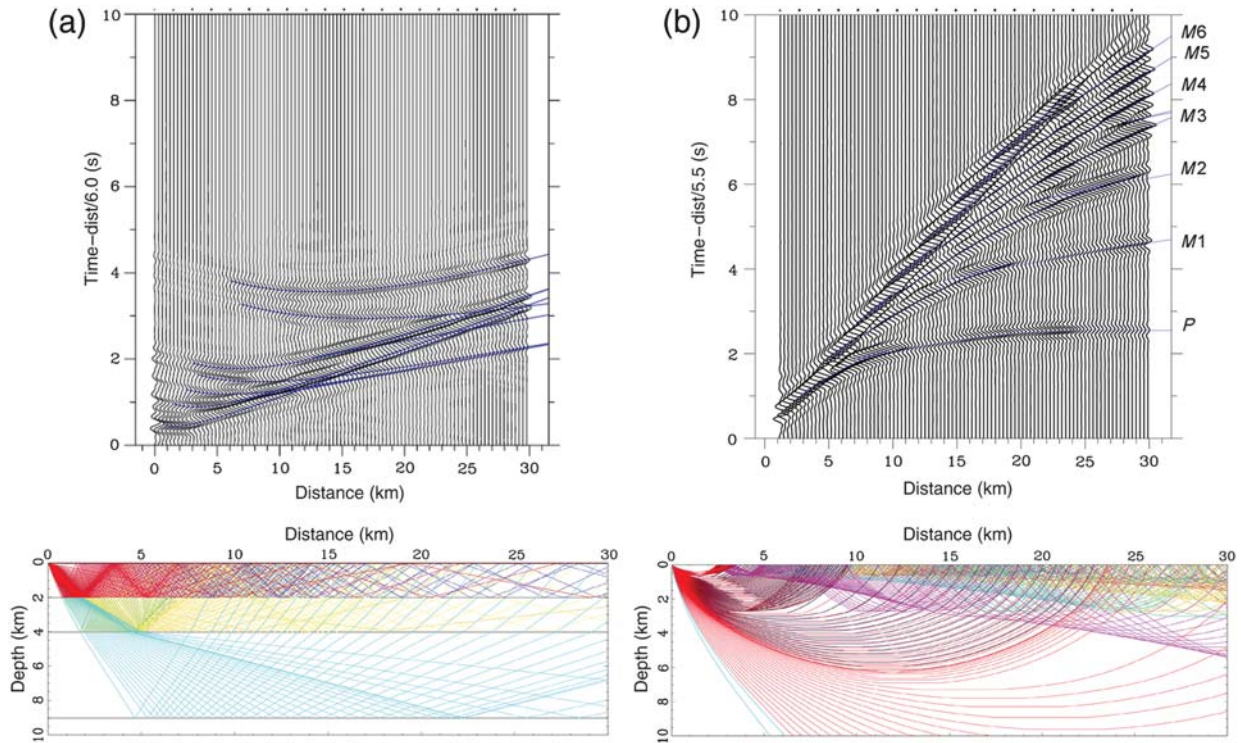
Figure 6. (a) Upper panel, synthetic seismograms and travel-time curves of refraction and reflection phases from a constant-velocity-layered model excited by a surface source. Lower panel, ray diagrams of corresponding refraction and reflection phases. A velocity of 6.0 km/s was used to reduce this time section. (b) Upper panel, synthetic seismograms and travel times of primary and multiple refractions from a layered steep-velocity-gradient model (Model-1D of Fig. 5) excited by a surface source; lower panel, ray diagrams of corresponding seismic phases. A velocity of 5.5 km/s was used to reduce this time section. Ray codes named as *P* for the primary refraction phase, *M*1 through *M*6 were the first through sixth free-surface multiples.
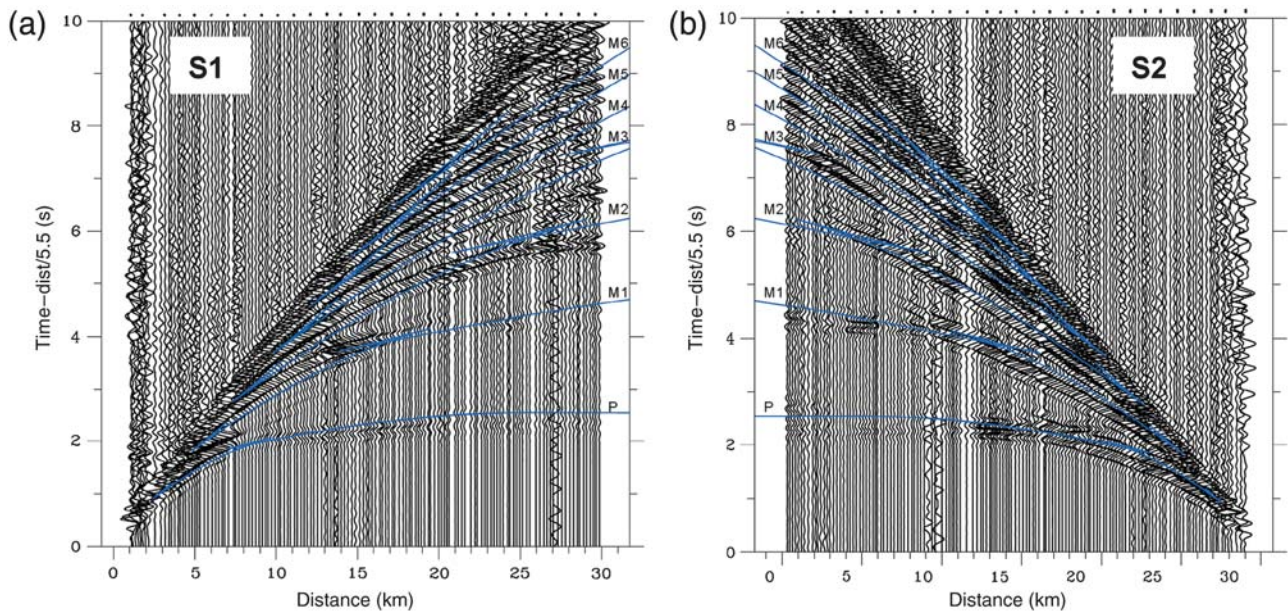

Figure 7. Trace of normalized recorded sections from shot points (a) S1 and (b) S2. Recorded sections of S1 are plotted on a distance coordinate system, with the shot point located at 0 km and distance from the shot point increasing toward the southeast direction of the seismic profile (Fig. 1). Recorded sections of S2 are also plotted on a distance coordinate system, with the shot point located at 30 km and distance from the shot point decreasing toward the northwest direction of the seismic profile (Fig. 1). Solid lines within both seismic sections are the travel-time curves of primary and multiple refractions, from a best-fit 1D model with steep velocity gradients (Model-1D of Fig. 5). A velocity of 5.5 km/s was used to reduce both time sections. Names of ray codes are the same as in Figure 6.
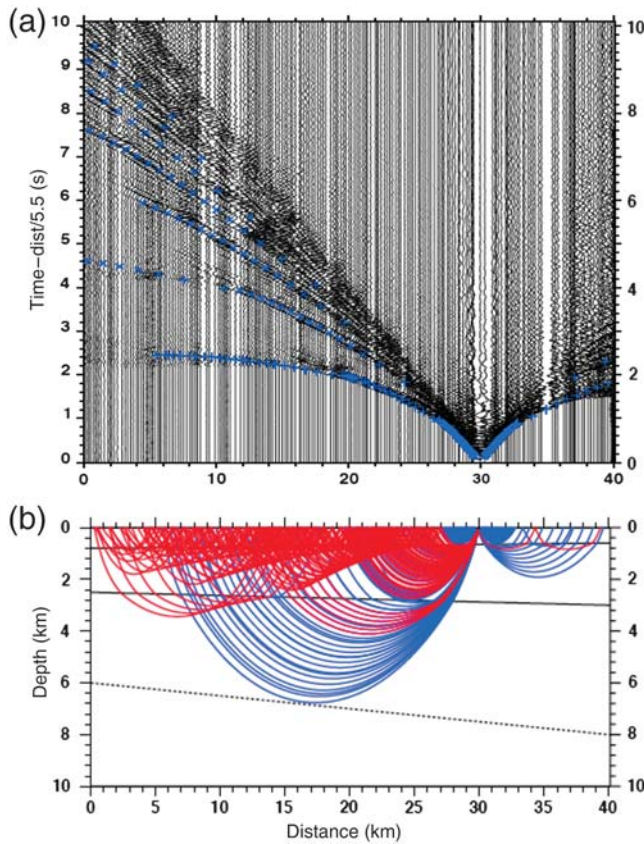
Figure 8. Recorded sections of S1 and travel times (cross symbols) computed by RAY84 (Luetgert, 1988) based on the 2D model proposed in this study. Shot point S1 is set at a distance of 10 km, increasing toward the southeast direction of seismic profile (Fig. 1). A velocity of 5.5 km/s was used to reduce the time section. (a) The first arrivals and multiples well fitted by the computed travel times. (b) Orientation and depth of the 2D layer model, and ray diagrams of first arrivals (blue traces) and multiples (red traces) from shot point S1. The dashed line in this model indicates the lower boundary of the sediment layer.

duration of shallow events, and thereby underestimate the risk posed by seismic hazards. Furthermore, the steep velocity gradient of the sediment layer would effectively bend any high-frequency seismic incident waves to the vertical direction as they approach the free surface, thereby complicating interpretations of seismic signals.

For example, we examined a shallow event (Fig. 11a) that occurred near the TAIGER shot point S1, to investigate the later phases recorded by a strong-motion array operated by the CWB (Shin, 1993). The later phases, thus noted as PP and PPP for vertical component and SS and SSS for two horizontal components, are clearly identified in one selected seismic record (Fig. 11b). We analyzed vertical- and two horizontal-component velocity waveforms from seismic stations located along an approximately north–south profile (Fig. 12). From those observations, clear later phases were observed along the profile, with amplitudes as large as those of the primary phases for both P wave and S wave. The present results indicate that well-developed, multiple diving
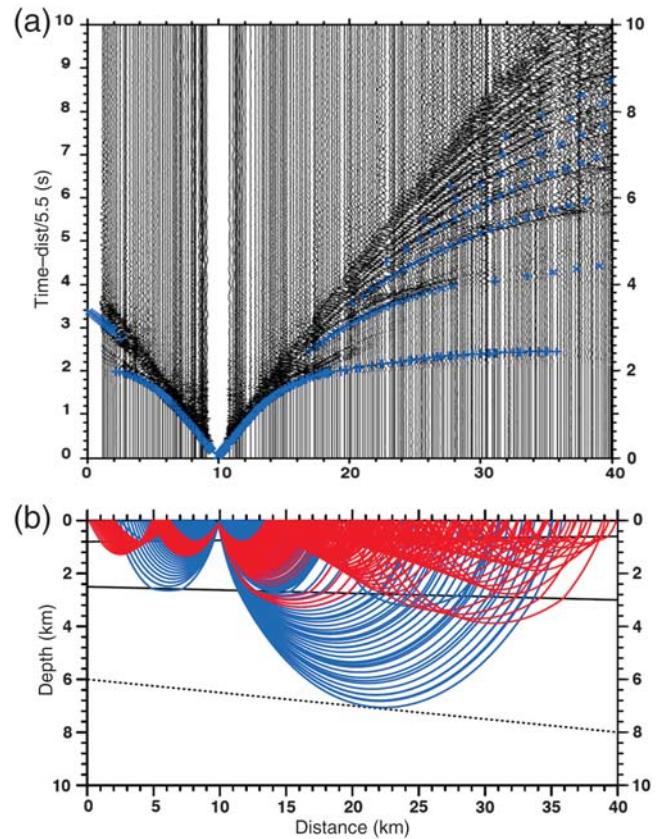
Figure 9. Recorded sections of S2 and travel times (cross symbols) computed by RAY84 (Luetgert, 1988) based on the 2D model proposed in this study. Shot point S2 is set at a distance of 30 km, increasing toward the southeast direction of seismic profile (Fig. 1). Others are the same as in Figure 8.
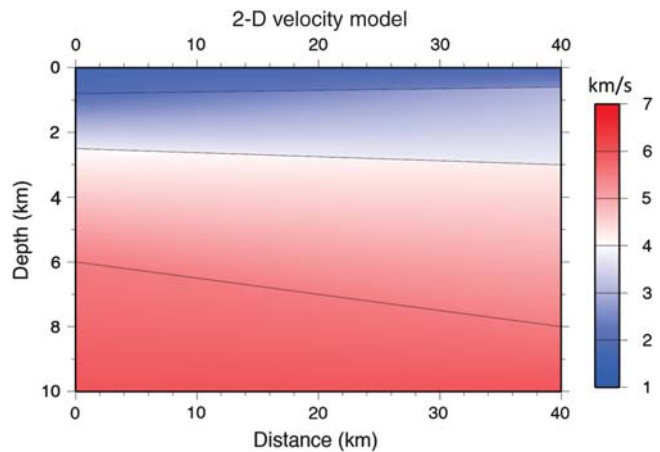

Figure 10. 2D P-wave velocity model determined in this study as the best fit for the travel times of seismic sections of shots S1 and S2. The shot points of S1 and S2 are located at the surface, at distances of 10 and 30 km in the model, respectively. The 2D model was constructed by a linear interpolation of the two 1D velocity profiles (Model-WEST and Model-EAST in Fig. 5).

waves propagated within the sediment layers with a steep velocity gradient. Thus, multiple diving waves are excited not only by surface explosions, but also by shallow
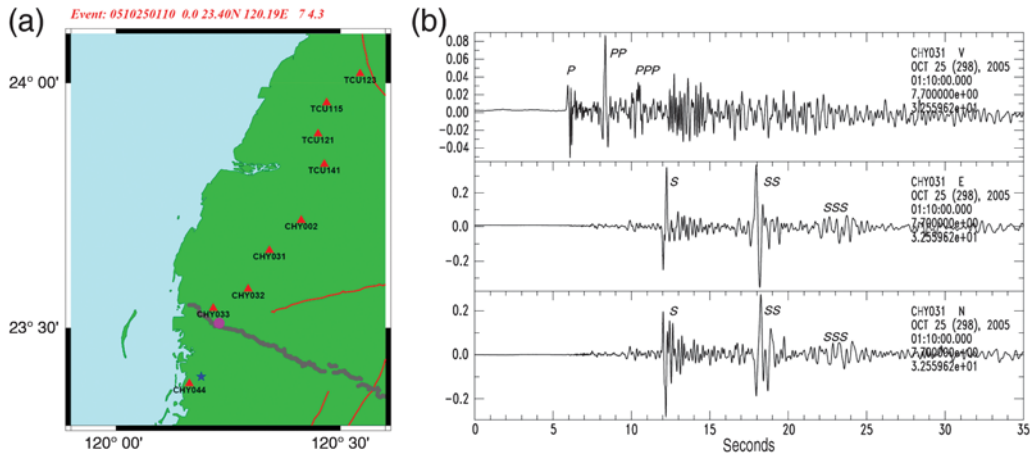
Figure 11. Normalized multiple diving waves recorded from a shallow earthquake in southwestern Taiwan (origin time: 25 October 2005; location: latitude 23.40° N, longitude 120.19° E, depth 7.0 km; M_L 4.3). (a) Star, location of the event; triangles with station codes, selected strong-motion stations that recorded the event. Pink circle, the location of the shot point S1; gray lines, the deployed seismic line of the TAIGER explosion experiment. (b) Recorded three-component velocity seismograms of this event from a seismic station (CHY031 in Fig. 11a). The vertical (V), east–west (EW), and north–south (NS) components are shown as the top, middle, and bottom traces, respectively. The seismic phases marked as *P*, *PP*, and *PPP* in vertical component were picked as direct *P* wave and its multiples; *S*, *SS*, and *SSS* in both horizontal components were picked as direct *S* waves and their multiples.
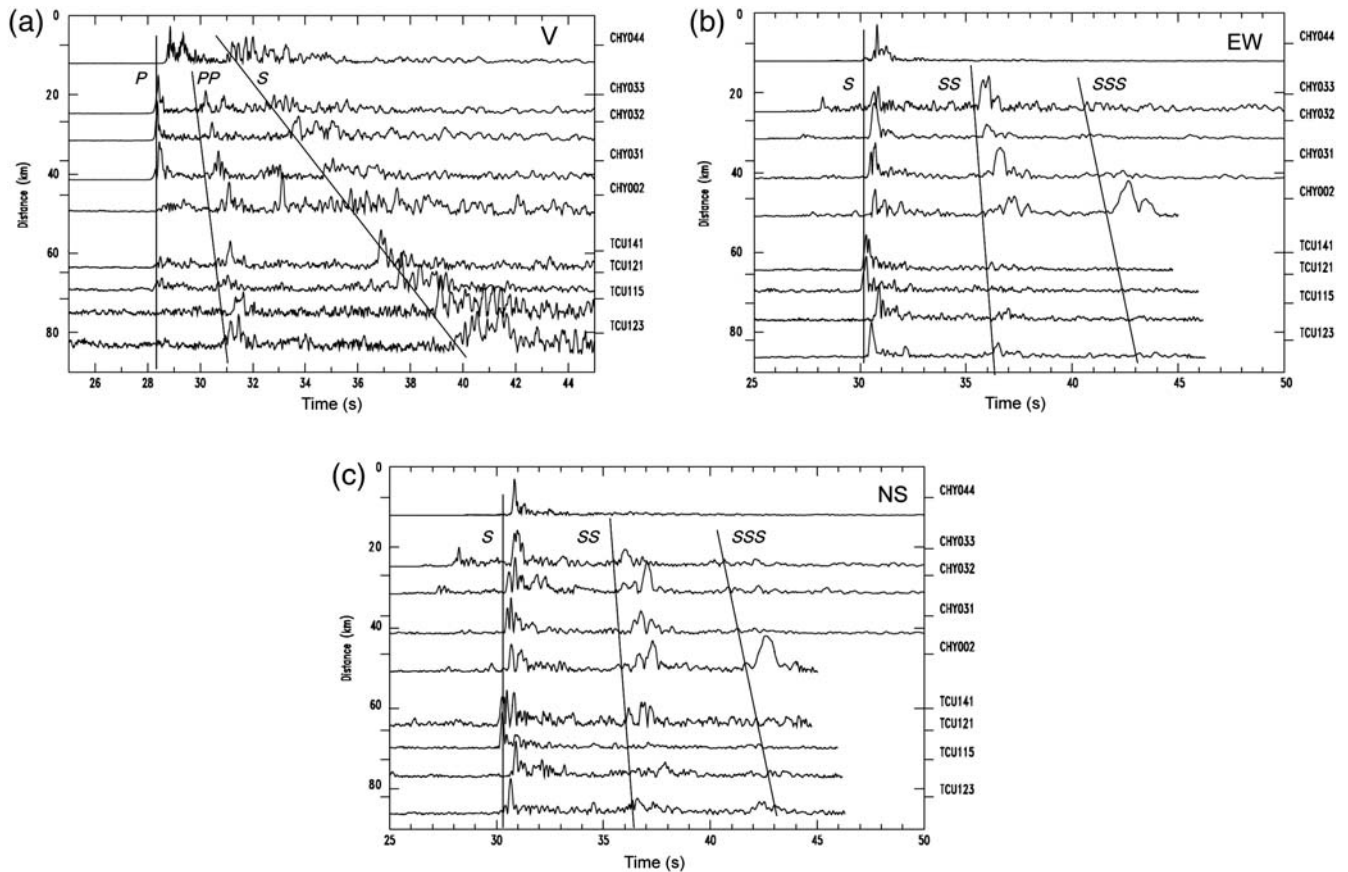

Figure 12. (a) Recorded vertical-component velocity seismograms shown as a seismic section in Figure 11. Each seismogram is enveloped and normalized to its peak value. A velocity of 6.0 km/s was used to reduce the time section. The travel-time curves *P* and *PP* represent the direct *P* wave and its multiple refractions, respectively. (b) Recorded east–west-component and (c) recorded north–south-component velocity seismograms shown as seismic sections in Figure 11. Each seismogram is enveloped and normalized to its peak value. The travel-time curves *S*, *SS*, and *SSS* represent the direct *S* wave and its multiple refractions, respectively. In both seismic sections, a velocity of 3.5 km/s was used to reduce the time section.

earthquakes. The multiple diving waves are observed not only from compression waves, but also from shear waves (Figs. 11 and 12). In fact, for local events, the ground-motion amplitudes of shear waves are usually larger than those of compression waves. Thus, an understanding of the propagation of multiple diving shear waves, and of the velocity profile of shear waves at shallow depths, would contribute significantly to the mitigation of seismic hazards.

In western Taiwan, the great thickness of cover sediments results in abnormally large amplitudes for short-period surface waves (Huang, Teng, *et al.*, 1996; Chung and Yeh, 1997; Hwang *et al.*, 2003). Information on shear waves at shallow depths is usually obtained by analyses of the dispersion of surface waves. No previous study has examined the shear-wave velocity gradient in an analysis of diving waves. Likewise, our analysis of seismic explosion data did not yield the shear-wave velocity gradients of the study region. To revise the *P*-wave model proposed by Chen (1995) for earthquake relocations and predictions of strong motions, it will be necessary to revise the corresponding sediment shear-wave gradient-velocity model. Additional observations from the TAIGER broadband seismic network and from the Taiwan strong-motion network are required to resolve this issue. Furthermore, the mitigation of seismic hazards requires 3D mapping of the basin and related 3D numerical modeling of wave propagation.

Conclusions

Seismic explosion data collected as part of the TAIGER project in the western coastal plain of Taiwan reveal high-energy later arrivals. These arrivals are identified as free-surface-reflected multiples induced by a steep velocity gradient at shallow depth. An accurate 2D layer-velocity model was constructed based on seismic-raytracing modeling. The survey area can be considered as a thick sediment layer dipping slightly to the east. The shallow part of the layer shows lateral variations, with increasing seismic velocities and gradients from west to east. The calculated velocity gradient for the thick sediment layer may require a revision of the regional seismic velocity model of southwestern Taiwan, in order to accurately locate local earthquakes and to predict strong ground motions that are likely to be associated with large earthquakes in the region.

Data and Resources

The data used in this research were collected by the TAIGER (TAiwan Integrated GEodynamics Research) project, the Institute of Earth Sciences, Academia Sinica, and the Central Weather Bureau. Data processing was performed using Seismic Analysis Code (SAC) 2000 (http://www.iris.edu/manuals/sac/manual.html; last accessed October 2012; Goldstein *et al.*, 2003) and PLOTSEC—Generalized Software for Seismic Refraction Data (http://www.eos.ubc.ca/personal/amor/plotsec/plotsec.html; last accessed October 2012). Some

figures were made using the Generic Mapping Tools (GMT) (http://www.soest.hawaii.edu/gmt; last accessed October 2012; Wessel and Smith, 1995).

Acknowledgments

References

Chapman, C. H. (1978). A new method for computing synthetic seismograms, *Geophys. J. Roy. Astron. Soc.* **54,** 481–518.

Chen, Y. L. (1995). Three-dimensional velocity structure and kinematic analysis in the Taiwan area, *Master's Thesis*, National Central University, Jungli, Taiwan.

Chung, J. K., and Y. T. Yeh (1997). Shallow crustal structure from short-period Rayleigh-wave dispersion data in southwestern Taiwan, *Bull. Seismol. Soc. Am.* **87,** 370–382.

Goldstein, P., D. Dodge, M. Firpo, and L. Minner (2003). SAC2000: Signal processing and analysis tools for seismologists and engineers, in *International Handbook of Earthquake and Engineering Seismology*, W. H. K. Lee, H. Kanamori, P. C. Jennings, and C. Kisslinger (Editors), chapter 85.5, Academic Press, San Diego, http://www.iris.edu/software/sac/ (last accessed October 2012).

Huang, B. S., K. C. Chen, and Y. T. Yeh (1996). Source parameters of the December 1993 Tapu earthquake from first-P motions and waveforms, *J. Geol. Soc. China* **39,** 235–250.

Huang, B. S., T. L. Teng, C. C. Liu, and T. C. Shin (1996). Excitation of short-period surface waves in Taiwan by the Hyogo-ken Nanbu earthquake of January 17, 1995, *J. Phys. Earth* **44,** 419–427.

Huang, B. S., C. Wang, D. Okaya, F. Wu, W. Liang, and W. Huang (2008). Observation for high velocity gradients in the western plain of Taiwan from TAIGER experiment (abstract T31C-2016), *Eos Trans. AGU* **89,** no. 53 (Fall Meet. Suppl.), T31C-2016.

Hwang, R. D., G. K. Yu, W. Y. Chang, and J. P. Chang (2003). Lateral variations of shallow shear-velocity structure in southwestern Taiwan inferred from short-period Rayleigh waves, *Earth Planets Space* **55,** 349–354.

Lin, A. T., A. B. Watts, and S. P. Hesselbo (2003). Cenozoic stratigraphy and subsidence history of the South China Sea margin in the Taiwan region, *Basin Res.* **15,** 453–478.

Luetgert, J. H. (1988). User's manual for RAY84/R83PLT interactive two-dimensional raytracing/synthetic seismogram package, *U.S. Geol. Surv. Open-File Rept. 88-238*, 52 pp.

McMechan, G. A., and W. D. Mooney (1980). Asymptotic ray theory and synthetic seismograms for laterally varying structure: Theory and application to Imperial Valley, California, *Bull. Seismol. Soc. Am.* **70,** 2021–2035.

Meissner, R. (1965). Multiple events in refraction shooting, *Geophys. Prospect.* **13,** 617–658.

Okaya, D., F. T. Wu, C. Y. Wang, H. Y. Yen, B. S. Huang, L. Brown, and W. T. Liang (2009). Joint passive/controlled source seismic experiment across Taiwan, *Eos Trans. AGU* **90,** 289–290.

Sarkar, D., P. R. Reddy, K. L. Kaila, and A. S. S. S. R. S. Prasad (1995). A research note on multiple diving waves and high-velocity gradients in the Bengal sedimentary basin, *Geophys. J. Int.* **121,** 969–974.

Shin, T. C. (1993). Progress summary of the Taiwan strong motion instrumentation program, in *Symp. on the Taiwan Strong Motion Instrumentation Program*, 1–10.

Teng, L. S. (1990). Geotectonic evolution of the late Cenozoic arc-continent collision in Taiwan, *Tectonophysics* **183,** 57–76.

Wang, C., D. Okaya, F. Wu, H. Yen, B. Huang, and W. Liang (2008). Diverse seismic imaging created by the seismic explosion experiment of the TAIGER project (abstract T33E-05), *EOS Trans. AGU* **89,** no. 53 (Fall Meet. Suppl.), T33E-05.

Wessel, P., and W. H. F. Smith (1995). A new version of the Generic Mapping Tools (GMT), *Eos Trans. AGU* **76,** 329.

Wu, F. T., L. L. Lavier, and TAIGER Teams (2007). Collision tectonics of Taiwan and TAIGER experiments (abstract T51A-0321), *EOS Trans. AGU* **88,** no. 52 (Fall Meet. Suppl.), T51A-0321.

Wu, F. T., W. T. Liang, J. C. Lee, H. Benz, and A. Villasenor (2009). A model for the termination of the Ryukyu subduction zone against Taiwan: A junction of collision, subduction/separation, and subduction boundaries, *J. Geophys. Res.* **114,** B07407, 16, doi: 10.1029/2008JB005950.

Institute of Earth Sciences
Academia Sinica
P.O. Box 1-55, Nankang
Taipei 11529, Taiwan
hwbs@earth.sinica.edu.tw
sjlee@earth.sinica.edu.tw
wtl@earth.sinica.edu.tw
    (B.S.H., S.-J.L., Y.-C.L., W.-T.L., W.-G.H.)

Institute of Geophysics
National Central University
No. 300, Jhongda Rd., Jhongli City
Taoyuan County 32001, Taiwan
wangcy@cc.ncu.edu.tw
    (C.Y.W.)

Department of Earth Sciences
University of Southern California
117 Zumberge Hall
3651 Trousdale Parkway, Los Angeles
California 90089-0740
okaya@usc.edu
    (D.O.)

Department of Geological Science and Environmental Studies
Binghamton University
Vestal Parkway, East Binghamton
New York 13902
francis@binghamton.edu
    (F.T.W.)